New Journal and we have not received input yet 22 (2021) 100857

Contents lists available at ScienceDirect

Thermal Science and Engineering Progress

journal homepage: www.sciencedirect.com/journal/thermal-science-and-engineering-progress

Flexible temperature sensor fabrication using photolithography technique

Husain Al Hashimi [a], Omar Chaalal [b,*]

[a] Consultant Mechanical Engineering, United Arab Emirates
[b] Abu Dhabi University College of Engineering, Chemical Engineering, United Arab Emirates

ARTICLE INFO

Keywords:
Adsorption
Conduction
Temperature
Sensor
Photolithography technique

ABSTRACT

With the ever-evolving demand for highly compact instruments, development in miniaturized products has been one of the major highlights in the technological research for the past century. A renowned example is the predictions given by Moore's law, pertaining to the proliferation in the numbers of transistors within electronic equipment's with time. Such devices found interest in several applications including industrial usages and biomedical fields, such as health diagnosis and therapies. Recent advances in electronic devices is related to its contact compatibility with non-planar surfaces, which are, otherwise, hard to scan with rigid devices. Such advancements were facilitated by the new developments in the electronic device's flexibility. In the current work, the fabrication of flexible sensor is provided in this paper, where a Nickel pattern along a polyimide substrate is used as a resistive based temperature indicator. One of the advantages of such sensors is its adaptability to various surface configurations, such as cylindrical tubes. Such sensor can play a crucial role in detailed examination of adverse flow condition, such as in phase change application, which can be achieved by its instantaneous measurement at multipoint resolution and conformity to non-planar surfaces

1. Introduction

In the past decades, developments in the sensor's fabrication have been the focus of wide of variety of applications. These include thermal actuator, flow rate and temperature measuring devices, and sensors pertaining to gas monitoring within food logistics [1–3]. Previous work focused on several temperature sensor types, which include resistive based sensors, thermistor, pyroelectric temperature sensors, and transistor-based temperature sensor. Several works [4–6] were involved in the development of flexible thermistors for skin surface monitoring applications. This was achieved with the introduction of novel materials such as poly(3,4-ethylenedioxythiophene) polystyrene sulfonate (PEDOT) and carbon allotropes. A temperature sensor with a sensitivity of 1.0% per °C was reported by Huang et al. [6]. Thermistor response time are in the order of seconds, which are generally inadequate for high frequency applications. Zinc Oxide (ZnO) nanowires utilized by Liao et al. [7] as a pyroelectric temperature sensor exhibited an improved response to thermistor-based temperature sensor, where the fabricated device was able to withstand a strain up 150% with a varying temperature sensitivity 39.3% and 16.8% per °C. A lower response time of 0.121 s was recorded by Sultana et al. [8]. Other work focused on the development of transistor-based temperature sensor [9,10], where a sensitivity of −24.2 mV/°C was reported for Single-wall carbon nanotubes (SWCNT) based temperature sensors. Organic field-effect transistor (OFET) flexible sensors were developed by Kim et al. [10], which was characterized with a bending radius of 1 cm. Complications in the transistor fabrication process places some restrictions in the mass production of such sensors. A review on the state of the art within flexible sensor fabrication is given by Costa et al. [11].

Several studies focused on developing high compact resistive sensor, with competitive spatial resolution performance. One such study is the works done by Xiao et al. [12], where they fabricated a flexible sensor based on thin platinum film, deposited on imidized polyimide layer. In Xiao et al. work, they were able to deduce the temperature coefficient of resistance (TCR) of the platinum sensor by direct resistance measurement over small temperature increment, from room temperature to 200 °C, where a value of 0.00291 $°C^{-1}$ was found for the sensor. From Xiao et al. work, they were able to conclude that a higher sensor's sensitivity and response frequency can be achieved by reducing parasitic heating loses, via thermal isolation enhancements, which was brought about by the flexible polyimide substrate, relative to the rigid silicon wafer [12]. In another study by Chia et al. [13], a platinum (Pt) temperature sensor was fabricated via "double sided fabrication process". Such approach involves depositing "serpentine shape" Pt metal sensor

* Corresponding author.
E-mail address: Omar.chaalal@adu.ac.ae (O. Chaalal).

https://doi.org/10.1016/j.tsep.2021.100857
Received 29 July 2020; Received in revised form 21 January 2021; Accepted 21 January 2021
Available online 27 January 2021
2451-9049/

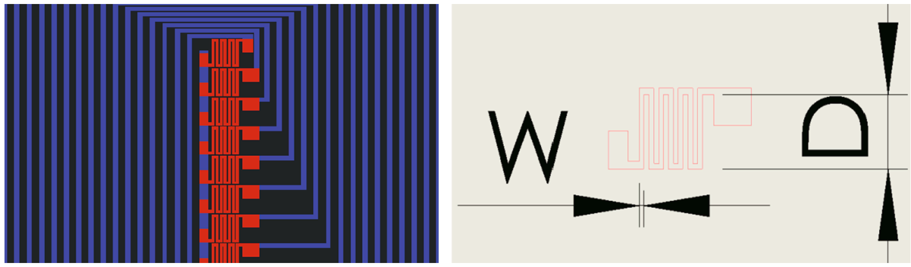

Fig. 1. Sensor design, (left) sensor pattern, (right) sensor design parameters.

on one of the polyimide, while patterning the scanning circuitry on copper clad laminated on the other side of polyimide sheet, establishing electrical connection through drilled holes within polyimide layer. Some of the sensor's design constrictions applied by Chia et al. was to ensure that resistance changes were due solely to the platinum sensor itself, which was achieved via dimensional manipulation of both Nickel (Ni) and copper pattern, a factor of direct influence upon the resistance value. A similar TCR value to Xiao et al. was report by Chia et al., which was deduced by observing the resistance variation relative to the ambient air thermocouple measurement [13].

In another work by Lee et al. [14,15], a flexible sensor was developed for the field of aerodynamics, so as to detect flow separation points over curved surface, via DC voltage measurements. The sensor was fabricated by engulfing a platinum-deposited sensor within a polyimide, which was temporarily attached to a rigid wafer, via a sacrificial Aluminum layer. The variation in thermal expansion properties, between the different layers in the platinum sensor, can lead to a crack failure within the sensor. Such issue can be averted by applying a low temperature control technique in the sensor's fabrication process, so as to compensate for the deviation in the thermal expansion properties between the polyimide and the platinum sensor [14,15]. The reported performance of the platinum flexible sensor was similar to the one acquired from the case with a rigid substrate, where a constant current circuit configuration was used for the excitation in order to prevent sensor self-heating. Like Xiao et al. [12] study, a high dynamical sensor response with a frequency as high as 160 kHz was observed within Lee et al. work, which they attributed it to the sensor's lower thermal inertia, due to thermal insulation brought about by flexible substrate.

Other kinds of flexible sensor include Humidity and chemical detecting sensors. An example of a humidity sensor is piezoelectric sensor, which utilizes Schottky junctions such as Platinum-Molybdenum DiSulfide ($Pt - MoS_2$) composite. Such sensors had a sensitivity around 35%/%RH, but fell short in terms of response time (92 s) [16,17]. On the other hand, chemical sensors can contain active sites that absorbs target molecules, which induces a measurable current flow, via electron-hole pair generation process. An example is the Tin (IV) Oxide (SnO_2)-functionalized MoS_2 chemical sensor, which absorbs oxygen molecules upon contact. A relatively high sensitivity (700%) was observed upon testing the sensor with Nitrogen dioxide gas [18].

Some of the major challenges with respect to the sensor's fabrication regard the dimensional scale difference between the patterned lead connection and the deposited sensor metal, which is one of the main causes for electrical disconnection, due to the sensor's breakage along the lead's edges. Such issues are further complicated if an adhesion layer exist between the flexible substrate and the pattern leads. From the aforementioned studies, it can be seen that it's crucial to include a thermal insulation within the metal sensor design, which can affect its performance criteria, such as measurement sensitivity and resolution [12–15,19]. In addition, the properties of the deposited metal sensor can be affected by the thickness of the deposited metal sensor, which some studies have indicated deviation from bulk metal value for thicknesses close to the mean free path. For instance, Siegel et al. [20] observed an inverse relation between resistance and temperature for gold thickness of several nm, as opposed to the proportion relation between resistance and temperature of gold bulkier thickness [20]. Annealing treatment to platinum sensor is recommended for TCR stability, where it tends to have an initial variation with temperature [14,15].

In the current work, the fabrication of a flexible temperature sensor is elaborated in this paper, along with prominent issues encountered at each step of the fabrication process. The flexible sensor consists of a thin film of Ni with copper (Cu) leads, which tends to overcome the adhesion issues arising within Pt-based sensor. An example is polyimide, where a tie coat is applied between the Pt and polyimide surface, which acts as an adhesion promoter. Such configuration can have a detrimental effect on the performance of platinum-based sensor. In fact, Lee et al. [14,15] have emphasized in their work that a lower TCR values for platinum sensor was acquired with the usage of Titanium tiecoat as an adhesion layer, which was associated with impurity introduction into the Pt layer [14,15]. Other advantages of Ni based sensor include hard, wear and corrosion resistance, as well as its ability to form a good adhesion with polyimide surface, via surface etching. In addition, Ni has a cheap price unlike other precious metals such as Pt [14,15,21,22].

2. Design and optimization

Fig. 1a shows an illustration of one of the sensor concept designs in which they are arranged in a column fashion. The design features sensors that are shifted towards the center, as shown in Fig. 1. Such configuration would provide symmetrical advantages; especially, in internal flow applications that can bring about a better flow integrity. The design contains 38 sensors that feature's 39 leads, including the ground lead, which is shared among all sensors. Ample spacing between the Positive terminal leads ensures transparency through the sensor, where 100 μm lead widths were separated by a distance of 200 μm spacing. The total width covered by the leads is 1.16 cm, with a maximum lead vertical length around 7.58 cm. Two parameters of the thin film resistor sensor can be readily deduced from Fig. 1, which includes the line width (w) and the line segment length (D).

The effect of the sensor array self-heating via the supplied current was investigated, where the temperature difference between the sensor's surface and the ambient was examined with respect to various sensor's geometrical parameters. Starting by Eq. (1), the convection heat transfer was assumed to be the main mechanism of heat transfer, while the sensor element resistance (R) is given by Pouillet's law, as shown in Eqs. (1) and (2), respectively.

$$I^2R = hA(T_s - T_\infty) \quad (1)$$

where I is the current, h is the heat transfer coefficient, A surface area of the sensor, and T_s *and* T_∞ are the surface and ambient temperatures, respectively.

$$R = \rho\frac{L}{wt} \quad (2)$$

where ρ is the sensor's resistivity, t is the sensor's thickness, and L is the total sensor's length, taken as the product of D by the number segment repetition (n). The heat transfer coefficient (h) was found from Nusselt's

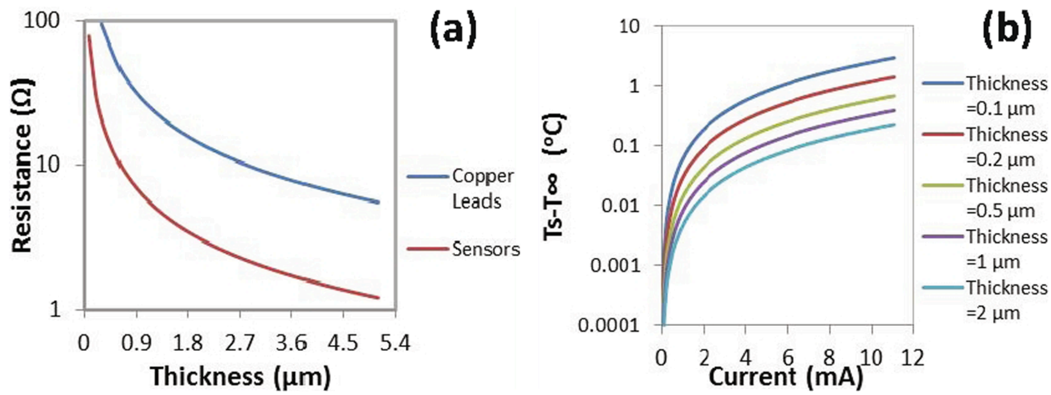

Fig. 2. Effect of deposition thickness upon sensors (a) Resistance, (b) Temperature change.

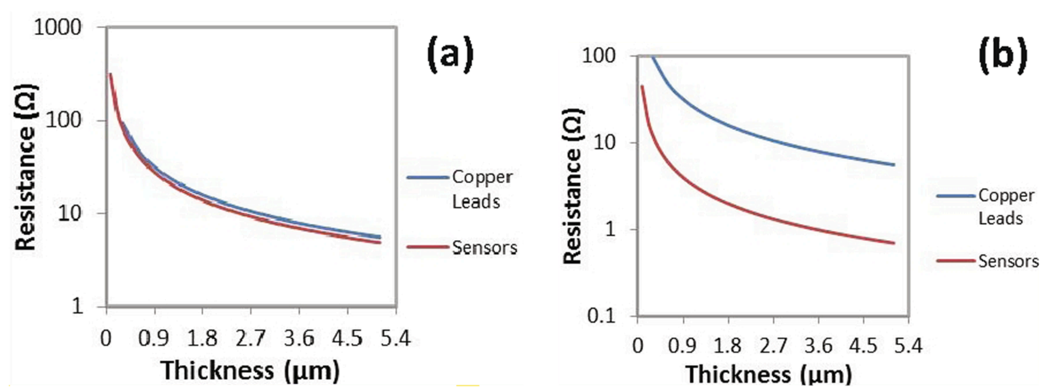

Fig. 3. Effect of Sensor line width upon its resistance (a) Sensor line width 15 µm, (b) Sensor line width 105 µm.

Number (Nu) correlation for free convection along horizontal plate, Eq. (3), where FC 72 working fluid properties was used to derive the Rayleigh Number [23]. The working fluid used is similar to the one used in Yerramilli et al. work [24]. X parameter in Eqs. (3) and (4) is the characteristic length of a flat plat, given by Eq. (5). The temperature difference- current relation, given by Eq. (7), was acquired from the heat transfer coefficient, Eq. (6), which was substituted in Eq. (1) and rearranged.

$$Nu = 0.27Ra_X^{1/4} = \frac{hX}{k_{fluid}} \tag{3}$$

$$Ra = \left[\left(\frac{g\beta}{\upsilon\alpha}\right)(T_s - T_\infty)X^3\right] \tag{4}$$

where β, υ, *and* α are the surrounding fluid properties, corresponding to thermal expansion coefficient, kinematic viscosity, and thermal diffusivity, respectively. The characteristic length in Eq. (4) can be found from Eq. (5).

$$X = \frac{A}{P} \tag{5}$$

where A and P are the area and the sensor's edge parameter length, respectively.

$$h = 538.741\left[\left(\frac{P}{A}\right)(T_s - T_\infty)\right]^{1/4} \tag{6}$$

$$T_s - T_\infty = \left(\frac{I^2R}{538.741A^{3/4}P^{1/4}}\right)^{4/5} \tag{7}$$

Fig. 2a shows the behavior of the sensor array resistance with respect to deposition thickness for Ni, where both the line width and the pitch

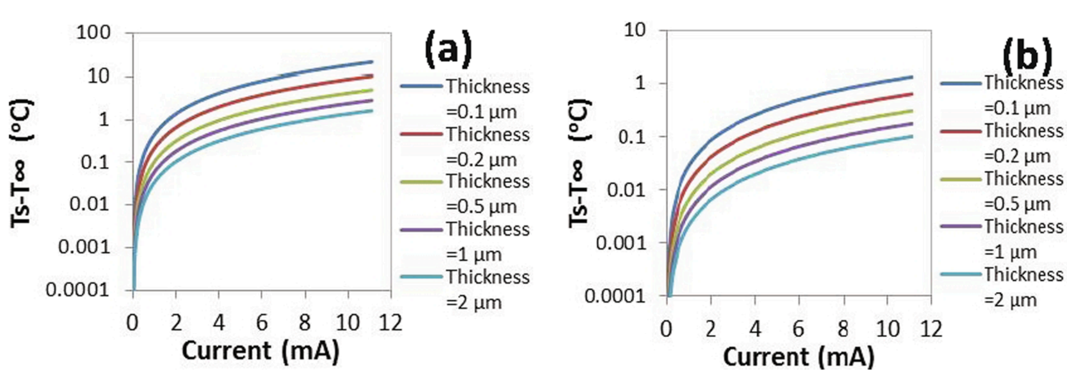

Fig. 4. Effect of Sensor line width upon its temperature change, (a) Sensors line width 15 µm, (b) Sensors line width 105 µm.

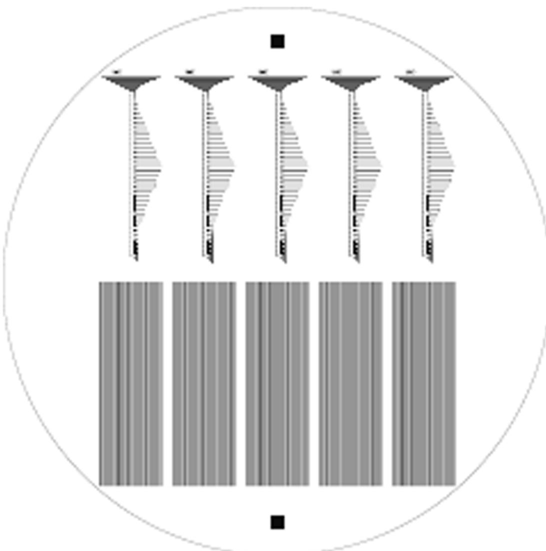

Fig. 5. Mylar film photomask.

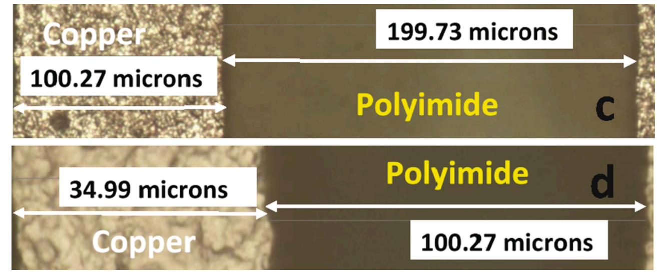

Fig. 6. Copper Lead patterns, (a) thinner width pattern feature relative to copper thickness, (b) Wider pattern feature relative to copper thickness, (c) biggest feature, (d) smallest feature.

spacing of the Ni pattern were 60 μm. A single line segment of the Ni pattern was chosen to have a length of 0.7 mm. In general, the material resistance decreases with deposition thickness. The resistance variation is within the same magnitude for both Ni and Cu leads. Such result is prominent beyond deposition thickness of around quarter of a μm, where the ratio between the Ni to Cu lead resistance change is 2:1. Such variation in resistance implies a requirement of thicker deposition on the leads, relative to the Ni layer. As for the temperature difference, between the sensor surface and the surrounding fluid, a similar conclusion can be drawn, where it decreases with respect to the deposition thickness, as shown in Fig. 2b. One of the relevant results concluded from Fig. 2b is the possibility to achieve less than 1 °C temperature using 10 mA or more of current, based on the deposited thickness of material. Another parameter that was examined in the analytical calculations is the line width of the sensor, as shown in Figs. 3 and 4. One aspect that merits line width increase of the sensor is the devices reliability, which tends to decrease with line width reduction, as noticed in a study by Yerramilli et al. [24]. A major disadvantage of using larger line width, however, is the large loss in the sensor's resistance, which can become comparable to the lead's resistance, as shown in Fig. 3. As a consequence, it may compromise the acquired data credibility, with the introduction of a comparable external resistance. Thus, a balance between electrical resistance and device reliability should be reached, to ensure a proper functionality in the testing measurement.

The Sensors temperature sensitivity can be acquired as follows: Starting with the temperature dependency of both the leads (R_L) and the sensor (R_S), the total resistance (R_T) can be found from Eq. (8).

$$R_T = R_S + R_L \tag{8}$$

Expanding Eq. (8) then simplifying common terms:

$$R_{So}[1+\alpha_s(T-T_o)] + R_{Lo}[1+\alpha_L(T-T_o)] = R_{So}[1+\alpha_s(T^{'}-T_o)] + R_{Lo} \tag{9}$$

$$\alpha_s R_{So} T + \alpha_L R_{Lo} T - \alpha_L R_{Lo} T_o = \alpha_s R_{So} T^{'} \tag{10}$$

A non-dimensional temperature fraction (θ) can be obtained through common terms rearrangement, which can be used as a measure for the sensor sensitivity, given by Eq. (11).

$$\theta = \frac{T-T^{'}}{T-T_o} = -\frac{\alpha_L R_{Lo}}{\alpha_s R_{So}} \tag{11}$$

For TCR ratio of the leads to sensor$\left(\frac{\alpha_L}{\alpha_s}\right)$ $\frac{1}{2}$:

$$\theta = \frac{T-T^{'}}{T-T_o} = -\frac{1}{2}\frac{R_{Lo}}{R_{So}} \tag{12}$$

The corresponding temperature fractions for a lead's thickness of 0.5 and 1 μm are 0.0308 and 0.0154, respectively, using 0.1 μm of Ni. In other words, the error involved in approximating the temperature changes with respect to Ni is around 3 and 1.5 percent, for a leads thickness of 0.5 and 1 μm, respectively.

3. Sensor fabrication

The sensor fabrication process begins with patterning the Cu leads for signal transmission purposes. This achieved via photolithography of a Cu clad laminated on a single a polyimide sheet, where a Dupont Pyralux sheet (AC 121200EM) was used. The Pyralux sheet consists of 12 μm of polyimide and 12 μm of Cu clad. The Pyralux sheet was mounted on a hollow fiberglass frame, where the patterned sensor can be easily removed from the frame upon its completion. A positive photoresist (Shipley 1813) was used to develop the pattern layer on the Pyralux sheet, where the exposed surface to the UV light would dissolve away upon developing. This was achieved using mylar film photomask, shown in Fig. 5, was used in the procedure, where the required lead pattern areas of the photoresist would be protected by the photomask from the UV light.

Upon photoresist development, the Pyralux sheet would be exposed to a chemical etchant, so as to acquire the needed copper pattern. Cupric chloride ($CuCl_2$) was initially used as an etchant, which was prepared by mixing hydrochloric acid (HCl) and hydrogen peroxide (H_2O_2). In principle, the HCl tends to react with the Pyralux copper clad, converting it in process to $CuCl_2$, a copper etchant. On the other hand, H_2O_2 tends to "reactivate" the $CuCl_2$ [25]. However, $CuCl_2$ tends to be a strong etchant agent of copper with a high etching rate. As a result, ferric chloride ($FeCl_3$), an industrial copper etchant, was used as an alternative etchant, which was capable of etching away 12 μm of Cu within 13 min. Another issue with chemical etching is the undercutting, which becomes more severe as the pattern width approaches the thickness of the sample to be etched, due to the isotropic nature of chemical etchant. To overcome the undercutting issue, a wider pattern leads were used, where copper leads were able to survive the chemical etching procedure, as shown in Fig. 6. Later on, the remaining photoresist would be washed away using acetone solvent after which the patterned Pyralux sheet has been cleaned and dried out.

Plasma treatment was applied to the patterned Pyralux sheet prior to the Ni pattern deposition, so as to increase its surface roughness. Therefore, a better surface adhesion to the deposited Ni would be achieved, via inter mechanical interlock. During plasma treatment, oxygen (O_2) gas was ionized at a power rating of 200 W. The chamber pressure was set around 60 mTorr, where the sample has been exposed to plasma for a duration of 300 s, as recommended by Woo et al. [26]. Two Ni deposition method was investigated: sputtering and electron beam evaporation. Ni metal deposited via sputtering resulted in a structure

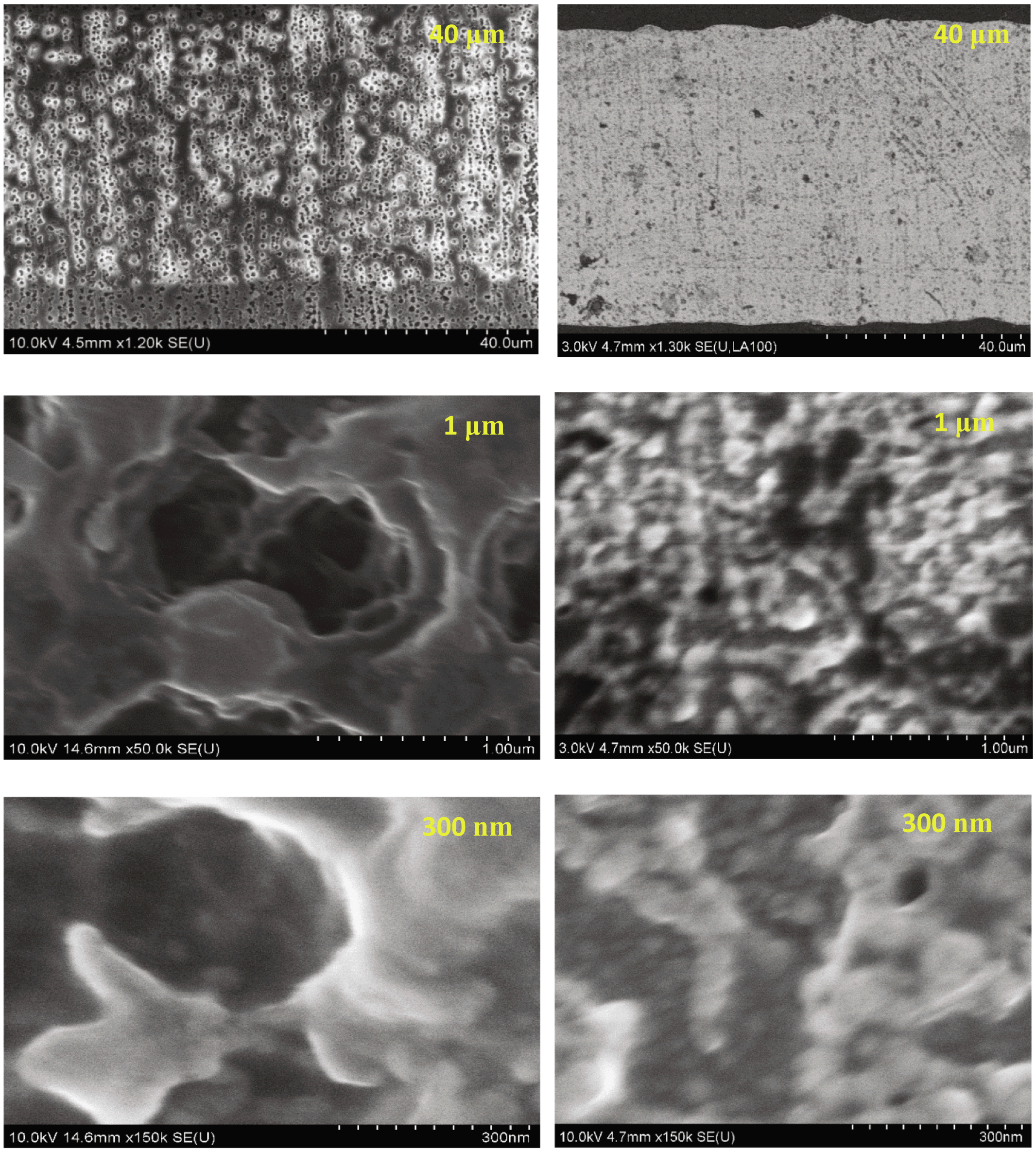

Fig. 7. SEM images for the two 50 nm Nickel film samples at different magnification, (Left column) continuous deposition, (Right column) intermittent deposition with cooling intervals.

with degraded conductivity. In a further study, two samples of Ni thin films of 50 nm thickness were deposited via sputtering, where their morphology were examined under scanning electron microscope (SEM). The sputtering machine was configured at 300 W, where argon gas was supplied at a flow rate of 5 sccm. One of the samples was continuously deposited to the required thickness, while the other sample was deposited at an interval of 3 min with a cool down time between deposition. The cool down time between depositions lasted for 10 min. Fig. 7 shows images from the SEM of the samples. The Ni sample that was deposited with a cool down time tend to form a conglomerate structure. On the other hand, the sensor that was continuously deposited showed signs of particle dispersion, as illustrated in Fig. 7. Such morphological structures have direct consequences upon the observed electrical conductivity of the sensor, where the sample that was deposited continuously showed null conductance, unlike the sample that was deposited with occasional cool down time periods. Despite the improvement brought about by the intermittent deposition, the acquired TCR along the thin film was still high, which was in the order of 0.0004 K^{-1} in some of the patterned Ni films.

Deposition via electron beam evaporation resulted in an appreciable TCR value, which were in the range of 0.001 K^{-1}–0.002 K^{-1}. Apparently, Ni metal deposited via electron beam evaporation has inherent conductivity advantages, which might be related to the directional orientation in the metal deposition, relative to sputtering deposition process. The degradation in the Ni thin film electrical conductivity can be correlated to the usage of argon as the ionizing gas rather than O_2, during the sputtering process. Previous studies by Guziewicz and et al. [27], Karpinski and et al. [28], and Angadi and Udachan [29] indicated that the grain size is affect by the O_2 content of the ionizing gas, which in turn has a direct impact upon the mean free path of the conduction electrons. As a consequence, the lack of O_2 during the sputtering deposition can bring about Ni dispersion, which would hamper the electrical conductivity along the deposited Ni film.

The Ni patterning is similar to the wet etching process of the Pyralux sheet from which the Cu leads were formed. In practice, a thin film layer of Ni with a thickness of 50 nm would be deposited on the Pyralux with patterned Cu leads, where a positive photoresist would be spin coated on top of the deposited Ni layer. Afterwards, another set of Mylar mask

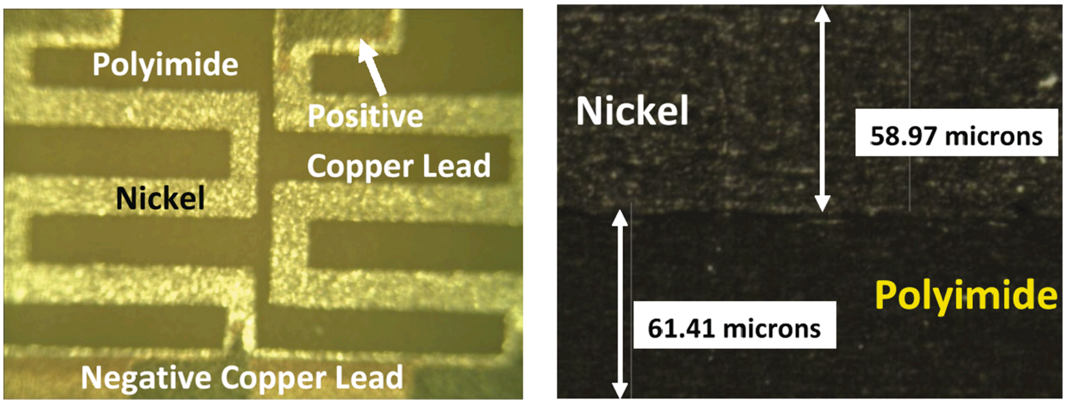

Fig. 8. Depiction of Nickel pattern on the copper leads (left) Nickel pattern via wet etching, (right) measured dimension.

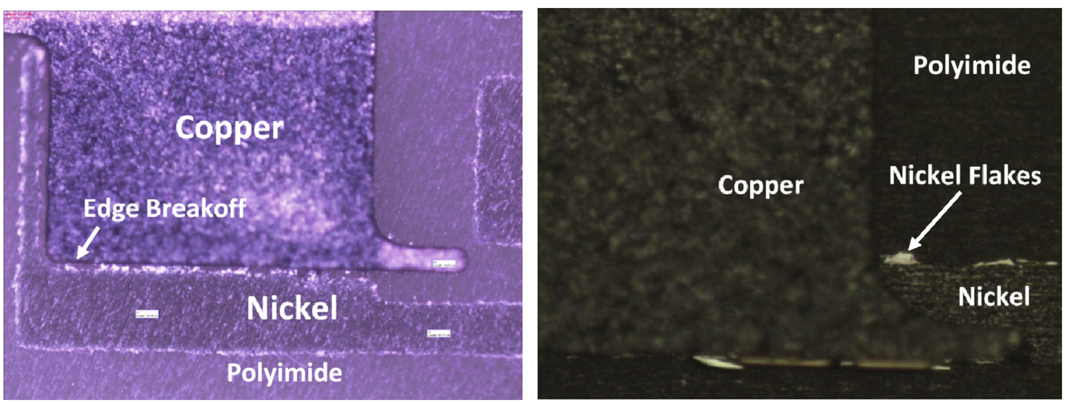

Fig. 9. Depiction of deposited Nickel contact with copper leads pattern using two different liftoff shadow mask, (left) Shipley 1813 photoresist, (right) AZ 4620 photoresist.

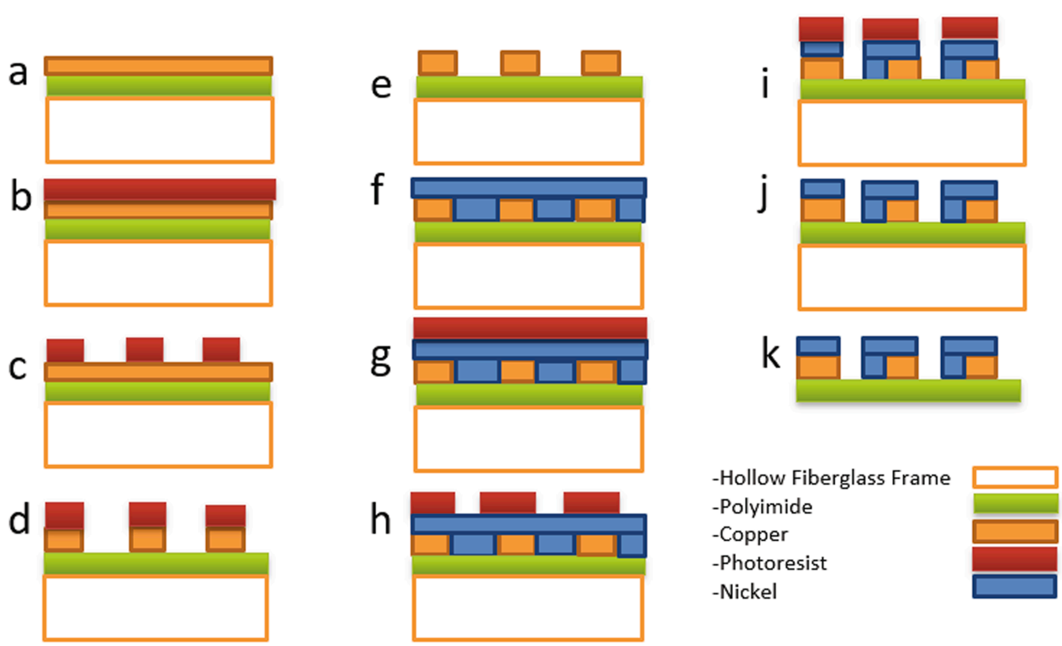

Fig. 10. Summary of Nickel Sensor fabrication.

would be used to control the UV exposure upon the photoresist, where the developer would expose the unwanted region of the Ni thin film. This step would pave the way for the Ni patterning, where the wet etching process would clear away the uncoated regions of the Ni thin film. Fig. 8 shows a depiction of the Ni pattern upon the Cu leads.

Ni patterning via photoresist shadow mask liftoff was also attempted,

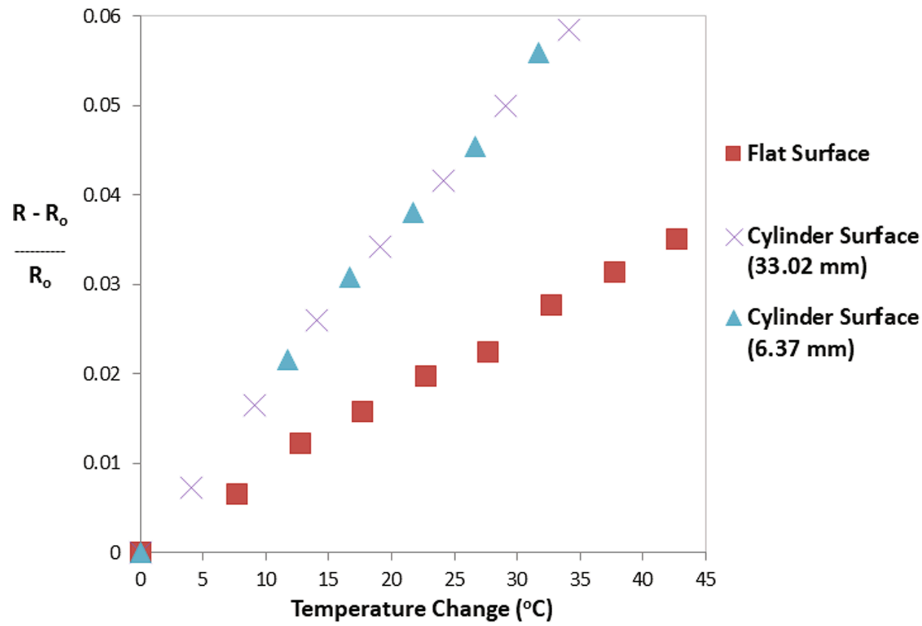

Fig. 11. Resistance fraction change versus temperature.

Table 1
TCR values.

Surface Geometry	TCR (k^{-1})
Flat	0.001
Cylinder (1.3 in.)	0.0017
Cylinder (6.37 mm)	0.0018

which was less stable in terms of its contact with the Cu leads. As shown in Fig. 9, the Ni pattern tend to break along the edge of the Cu lead, which would result in a signal disconnection. Using a thicker shadow mask, such as the AZ 4620, can relief the structural stress during liftoff, where a better contact is achieved between the Ni and the Cu leads, as shown in Fig. 9. Overall, the measured resistance of the sensor pattern was more consistent using wet etching than shadow mask liftoff technique, where tiny flakes of Ni appear along the edge of the pattern after liftoff technique, as shown in Fig. 9.

Fig. 10 summarizes the entire Ni thin film sensor fabrication process. The figure is not to scale.

4. Sensor characterization

The performance of the patterned sensor was characterized over different surface geometries, which include flat and various cylindrical surfaces with different diameters. Fig. 11 plots the fractional resistance change of the nickel sensor as a function of the sensor's temperature change, with respect to its initial temperature. As shown in Fig. 11, a similar fractional change in resistance with temperature is acquired using cylindrical geometries with different diameters. The acquired TCR values for both cylinders was close to 0.002 K^{-1}, as shown in Table 1. Comparing TCR values acquired by the Ni sensor on flat surface and both cylindrical surfaces, the TCR value was higher in the latter case, which might be related to structural rearrangement of the Ni thin film. Effectively, a higher sensitivity is achieved by the Ni sensor on non-planar surfaces

5. Conclusions

In the current work, details for fabrication of flexible temperature sensors were provided in this paper, where the encountered obstacles within each step of sensor patterning was examined, with respect to various deposition and patterning techniques. For instance, issues associated with Cu leads undercutting were rectified via patterning width variation, with respect to the deposited Ni thickness. While wet etching patterning resulted in a better morphology of the Ni thin film, relative to liftoff techniques. The dissociated conductivity properties of the sputtered Nickel thin film were attributed to the ionizing medium, where previous studies observed that sputtered Ni films within an O_2 environment can benefit with respect to its electrical properties. As for the observed TCR values of the patterned Ni sensor, a similar value was acquired for different cylindrical diameters, which was higher than the value attained for planar surfaces.

Declaration of Competing Interest

The authors declare that they have no known competing financial interests or personal relationships that could have appeared to influence the work reported in this paper.

References

[1] Q. Chen, X. Luo, S. Zhou, S. Liu, Dynamic junction temperature measurement for high power light emitting diodes, Rev. Sci. Instrum. 82 (2011).
[2] G. Kaltsas, et al., A novel microfabrication technology on organic substrates – application to a thermal flow sensor, J. Phys. Conf. Ser. 92 (2007), https://doi.org/10.1088/1742-6596/92/1/012046.
[3] E. Abad, B. Mazzolai, A. Juarros, A. Mondini, A. Krenkow, T. Becker, Fabrication and Encapsulation Processes, Radio Frequency Identification Fundamentals and Applications, Design Methods and Solutions, 2010, pp. 237–251, ISBN: 978-953-7619-72-5.
[4] S. Hong, Y. Lee, H. Park, S. Jin, Y. Jeong, J. Yun, I. You, G. Zi, J. Ha, Stretchable active matrix temperature sensor array of polyaniline nanofibers for electronic skin, Adv. Mater. 28 (2016) 930–935.
[5] B. An, S. Heo, S. Ji, F. Bien, J. Park, Transparent and flexible fingerprint sensor array with multiplexed detection of tactile pressure and skin temperature, Nat. Commun. 9 (2018).
[6] Y. Huang, X. Zeng, W. Wang, X. Guo, C. Hao, W. Pan, P. Liu, C. Liu, Y. Ma, Y. Zhang, et al., High-resolution flexible temperature sensor based graphite-filled polyethylene oxide and polyvinylidene fluoride composites for body temperature monitoring, Sens. Actuators, A 278 (2018) 1–10.
[7] X. Liao, Q. Liao, Z. Zhang, X. Yan, Q. Liang, Q. Wang, M. Li, Y. Zhang, A highly stretchable ZnO@fiber-based multifunctional nanosensor for strain/temperature/UV detection, Adv. Funct. Mater. 26 (2016) 3074–3081.
[8] A. Sultana, M.M. Alam, T.R. Middya, D. Mandal, A pyroelectric generator as a self-powered temperature sensor for sustainable thermal energy harvesting from waste heat and human body heat, Appl. Energy 221 (2018) 299–307.

[9] C. Zhu, A. Chortos, Y. Wang, R. Pfattner, T. Lei, A. Hinckley, I. Pochorovski, X. Yan, J. To, J. Oh, et al., Stretchable temperature-sensing circuits with strain suppression based on carbon nanotube transistors, Nat. Electron. 1 (2018) 183–190.
[10] D. Kim, T. Trung, B. Hwang, J. Kim, S. Jeon, J. Bae, J. Park, N. Lee, A sensor array using multi-functional field-effect transistors with ultrahigh sensitivity and precision for bio-monitoring, Sci. Rep. 5 (2015).
[11] J. Costa, F. Spina, P. Lugoda, L. Garcia, D. Roggen, N. Münzenrieder, Flexible sensors—from materials to application, Technologies 7 (35) (2019).
[12] S. Xiao, L. Che, X. Li, Y. Wang, A cost-effective flexible MEMS technique for temperature sensing, Microelectron. J. 38 (2007) 360–364, https://doi.org/10.1016/j.mejo.2007.01.022.
[13] B. Chia, et al., Temperature Sensor Array Using Flexible Substrate, MEMS, Kobe, Japan, 2007.
[14] G. Lee, F. Huang, C. Lee, J. Miau, A new fabrication process for a flexible skin with temperature sensor array and its application, ACTA Mech. Sin. 20 (2) (2004). ISSN: 0567-7718.
[15] G. Lee, J. Wu, J. Miau, A new fabrication process for a flexible skin with temperature sensor array, J. Chin. Inst. Eng. 25 (6) (2002) 619–625.
[16] J. Guo, R. Wen, Y. Liu, K. Zhang, J. Kou, J. Zhai, Z. Wang, Piezotronic effect enhanced flexible humidity sensing of monolayer MoS_2, ACS Appl. Mater. Interfaces 10 (2018) 8110–8116.
[17] D. Burman, S. Santra, P. Pramanik, P. Guha, Pt decorated MoS_2 nanoflakes for ultrasensitive resistive humidity sensor, Nanotechnology 29 (2018), 115504.
[18] Y. Kang, S. Pyo, D. Baek, J. Kim, Flexible and transparent NO_2 sensor using functionalized MoS_2 with light-enhanced response. Proceedings of the 2017 19th International Conference on Solid-State Sensors, Actuators and Microsystems, Kaohsiung, Taiwan, 2017.
[19] A. Petropoulos, D. Goustouridis, T. Speliotes, G. Kaltsas, Demonstration of a new technology which allows direct sensor integration on flexible substrates, Eur. Phys. J. Appl. Phys. 46 (2009) 1, https://doi.org/10.1051/epjap/2009020.
[20] J. Siegel, O. Lyutakov, V. Rybka, Z. Kolská, V. Švorčík, Properties of gold nanostructures sputtered on glass, Nanoscale Res. Lett. 6 (2011) 96.
[21] A. Yusoff, M. Syahrul, K. Henkel, Film adhesion in amorphous silicon solar cells, Bull. Mater. Sci. 30 (4) (2007) 329–331.
[22] Nickel as a Coating Material, Materion Brush Performance Alloys: Technical Tidbits, No. 34, 2011.
[23] I. Mudawar, T. Anderson, Parametric investigation into the effects of pressure, subcooiing, surface augmentation and choice of coolant on pool boiling in the design of cooling systems for high-power-density electronic chips, J. Electron. Packag. 112 (1990) 375.
[24] J. Myers, V. Yerramilli, S. Hussey, G. Yee, J. Kim, Time and space resolved wall temperature and heat flux measurements during nucleate boiling with constant heat flux boundary conditions, Int. J. Heat Mass Transf. 48 (2005) 2429–2442, https://doi.org/10.1016/j.ijheatmasstransfer.2004.12.050.
[25] Stop Using Ferric Chloride Etchant! (A Better Etching Solution), Instructables, Autodesk Inc, online Document, available at: http://www.instructables.com/id/Stop-using-Ferric-Chloride-etchant!–A-better-etc/step6/Alternative-overly-complex-Method-Make-Cupric-Chlo/.
[26] T. Woo, I. Park, K. Jung, W. Jeon, K. Seol, Effect of RF sputtering power on the adhesion of Ni thin film to polyimide, Electron. Mater. Lett. 7 (4) (2011) 353–358, https://doi.org/10.1007/s13391-011-0270-0.
[27] M. Guziewicz, et al., Electrical and optical properties of NiO films deposited by magnetron sputtering, Opt. Appl. XLI (2) (2011).
[28] A. Karpinski, et al., Deposition of nickel oxide by direct current reactive sputtering, Thin Solid Films 520 (2012) 3609–3613.
[29] M.A. Angadi, L.A. Udachan, Electrical properties of thin nickel films, Thin Solid Films 79 (1981) 149–215.